

Probing the effects of primordial black holes on 21-cm EDGES signal along with interacting dark energy and dark matter - baryon scattering

Ashadul Halder*

*Department of Physics, St. Xavier's College, 30,
Mother Teresa Sarani, Kolkata-700016, India.*

Madhurima Pandey†

*Theory Division, Saha Institute of Nuclear Physics,
HBNI, 1/AF Bidhannagar, Kolkata-700064, India.
Department of Physics, School of Applied Sciences and Humanities,
Haldia Institute of Technology, Haldia, West Bengal, 721657, India.*

Abstract

21-cm radio signal has emerged as an important probe in investigating the dark age of the Universe (recombination to reionization). In the current analysis, we explore the combined effects of primordial black holes (PBH), cooling off of the baryonic matter due to dark matter (DM) - baryon collisions and interaction of dark matter - dark energy (DE) fluid on the 21-cm brightness temperature. The variation of brightness temperature shows remarkable dependence on DM mass (m_χ) and the dark matter - baryon scattering cross-section (σ_0). Bounds in m_χ - σ_0 parameter space are obtained for different possible PBH masses and for different interacting dark energy (IDE) models. These bounds are estimated based on the observed excess (-500^{+200}_{-500} mK) of 21-cm brightness temperature by EDGES experiment. Eventually, bounds on PBH mass is also obtained for different values of dark matter mass and for different IDE model coupling parameters. The compatibility of the constraints of the IDE models, in the estimated bounds are also addressed.

Keywords: cosmology: dark ages, reionization, first stars; cosmology: dark energy; cosmology: dark matter; black hole physics

I. INTRODUCTION

The 21-cm cosmology is turning out to be a promising tool in understanding the dynamics of the early Universe. The redshifted signature of the 21-cm neutral hydrogen spectrum opens up a new window to understand the process of reionization and the factors in the early Universe

* ashadul.halder@gmail.com

† madhurima0810@gmail.com

influencing the same. Thus, study of the 21-cm line in reionization era helps in understanding several cosmological and astrophysical processes that might have contributed to the physics of the early Universe.

The 21-cm (~ 1.42 GHz) hyperfine spectrum is originated due to the transition between two spin states ($s = 0$ and 1) of the neutral H atoms. The hydrogen occupies around 75% of the entire baryonic mass of the Universe. The corresponding spin temperature indicates the population of hydrogen atoms with different energy states. The “Experiment to Detect the Global Epoch of Reionization Signature” (EDGES) [1] reported 21-cm absorption spectra at the cosmic dawn era ($14 < z < 20$) and predicted the 21-cm brightness temperature to be -500^{+200}_{-500} mK with 99% confidence level (C.L.). This measured brightness temperature is lower than the expected value.

The 21-cm brightness temperature T_{21} is related to the temperature difference $T_s - T_\gamma$, where T_s is the spin temperature and the T_γ is the background temperature (CMB temperature). The observed additional cooling of T_{21} by EDGES experiment can be realized by either enhancing the background temperature T_γ or by lowering the matter temperature which is equal to T_s at that epoch. Dark matter (DM) interactions such as the scattering of dark matter off baryons, dark matter annihilation or decay can inject energy into the background resulting in the rise in background temperature. There can be other processes such as possible dark matter - dark energy interaction, which can induce the larger than expected difference of T_s and T_γ . In this work, both these possibilities are explored. In addition, the possibility that the evaporation of Primordial Black Holes (PBHs) injecting more energy into the system is also addressed in this work.

PBHs [2–5] are believed to be formed during the radiation dominated era. PBHs forms due to the collapse of an overdensity region characterized by the size of the region which should be greater than the Jeans length R_j , where $R_j = \sqrt{\frac{1}{3G\rho}}$. Also the condition of the PBH formation is $\delta_{\min} \leq \delta \leq \delta_{\max}$, where δ is the density contrast. The maximum and minimum density contrast δ_{\max} and δ_{\min} respectively are governed by the value of $\delta\rho$, where the density $\rho = \rho_c + \delta\rho$, ρ_c being the critical density for collapse and δ_{\min} is the threshold of PBH formation. Moreover, there are several mechanisms describing the formation of PBHs [6–18]. In the work of [19], the masses of the PBHs $\geq 10^{15}$ g are adopted. But in the present work, we investigate the 21-cm signal with the PBH masses $10^{13} \leq \mathcal{M}_{\text{BH}} \leq 10^{14}$ g. This range of PBH mass is also considered in [20].

As mentioned earlier in this work, we address the possible influences of the factors namely DM - baryon scattering, possible DM - DE interaction [21–26] and the evaporation of PBH [19, 20, 27–31] simultaneously on 21-cm EDGES signal in the epoch of ignition of first star. The heating effect by the PBHs are assumed to be contributed by Hawking Radiation from PBH only. For the DM -

DE interaction three interacting dark energy (IDE) models given in [32] are chosen. The influence of DM - DE interaction on 21-cm signal has been discussed earlier in [32, 33]. Moreover, DM-DE interaction is discussed in several context such as in addressing the cosmological coincidence problem [34], Hubble tension [35], Large Scale Structure formation [36] etc.

The general form of the velocity dependent cross-section is given by $\bar{\sigma} = \sigma_0(v/c)^n$, where the index n depends on different physical dark matter processes and c is the velocity of light in space (in natural unit $\bar{\sigma} = \sigma_0 v^n$). In the case of DM with magnetic and/or electric dipole moment $n = +2, -2$ are considered. $n = 2, 1, 0, -1$ are applicable for scattering in presence of Yukawa potential [37], $n = -4$ is attributed for millicharged DM [38, 39]. In Ref. [40] the nature of the DM-baryon cross-section is discussed for a wide mass range of dark matter. Similar investigations are also carried out in Ref. [41–44]. In the present work, the dark matter - baryon interaction cross-section ($\bar{\sigma}$) is parameterized as $\bar{\sigma} = \sigma_0 v^{-4}$ [33, 45, 46]. The term σ_0 is the dark matter scalar scattering cross-section with baryons (of the type $\alpha_q \bar{\chi} \chi \bar{q} q$ for dark dark matter particle χ with coupling α_q). It may be mentioned in some earlier works [42, 43] millicharged dark matter is considered. But here, we assume a particle dark matter candidate and adopt value of $\sigma_0 \sim 10^{-41} \text{cm}^2$ consistent with the scalar cross-section bound obtained from ongoing direct dark matter search experiments (extrapolating the allowed region for $0.1 \text{ GeV} \leq m_\chi \leq 3 \text{ GeV}$ from recent experiments [47–49]) in the mass range discussed in this work. Several recent investigations on EDGES 21-cm signal also suggest the similar velocity dependence ($n = -4$) of the cross-section [45, 46, 50]. Moreover, $n = -4$ is chosen in many dark matter related cases namely hadronically interacting DM, millicharge DM, the Baryon Acoustic Oscillations (BAO) signal etc.

The paper is organized as follows. In Section II, we address the interaction between dark matter and dark energy and its effect in cosmic evolution. Section III deals with the injection by the PBHs in the form of Hawking radiation. In Section IV, the formalism of evolutions of various temperatures such as T_χ, T_b (DM temperature, baryon temperature) along with the effect of PBH evaporation are described. Section V describes the formalism for 21-cm absorption line. Calculations and results are shown in Section VI. Finally in Section VII, some concluding remarks are given.

II. DARK MATTER - DARK ENERGY INTERACTION

The DM - DE interaction may have a profound effect in the universal dynamics and hence on the optical depth and spin temperature of the 21-cm transition. In standard cosmological model,

TABLE I. Stability conditions of the model parameters for different IDE models

Model	\mathcal{Q}	EOS of dark energy	Constraints
I	$3\lambda H(z)\rho_{\text{de}}$	$\omega < -1$	$\lambda < -2\omega\Omega_\chi$
II	$3\lambda H(z)\rho_\chi$	$\omega < -1$	$0 < \lambda < -\omega/4$
III	$3\lambda H(z)(\rho_{\text{de}} + \rho_\chi)$	$\omega < -1$	$0 < \lambda < -\omega/4$

the density parameters of dark matter (Ω_χ) and dark energy (Ω_{de}) are assumed to be evolved as $\Omega_{\chi,0}(1+z)^3$ and $\Omega_{\text{de},0}(1+z)^{3(1+\omega)}$ where, $\Omega_{\chi,0}$ and $\Omega_{\text{de},0}$ are the respective density parameters at $z=0$ and ω is the equation of state (EOS) parameter of dark energy. However, if the interaction between dark matter and dark energy is taken into account, the evolution of dark matter and dark energy densities take the forms [32],

$$(1+z)H(z)\frac{d\rho_\chi}{dz} - 3H(z)\rho_\chi = -\mathcal{Q} \quad (1)$$

$$(1+z)H(z)\frac{d\rho_{\text{de}}}{dz} - 3H(z)(1+\omega)\rho_{\text{de}} = \mathcal{Q} \quad (2)$$

where \mathcal{Q} denotes the energy transfer between dark matter and dark energy due to DM-DE interaction. In the present work, we consider three benchmark models in order to investigate the effect of DM - DE interaction in the brightness temperature. The energy transfer expressions of those benchmark models are described below [51–54].

$$\text{Model-I} \quad \mathcal{Q} = 3\lambda H(z)\rho_{\text{de}}$$

$$\text{Model-II} \quad \mathcal{Q} = 3\lambda H(z)\rho_\chi$$

$$\text{Model-III} \quad \mathcal{Q} = 3\lambda H(z)(\rho_{\text{de}} + \rho_\chi)$$

Here, λ is the coupling parameter, which determine the strength of the dark matter - dark energy interaction. The stability conditions for each of the models are described in Table I. Several phenomenological studies have been carried out with observational data of PLANCK, Supernova Ia (SNIa) Baryon Acoustic Oscillation (BAO) [53–60] yielding the constraints for different models (in Table II). It is to be mentioned that, all the IDE models discussed in this section are independent of the dark matter - baryon interaction.

III. EFFECT OF PRIMORDIAL BLACK HOLE

The energy injection of PBHs in the form of Hawking radiation [61] can be a possible source for heating up of the medium before the reionization. It has been shown by [19] that, in 21-cm scenario, the Hawking radiation is equally significant as that of the DM decay.

TABLE II. Constraints of the different IDE models

Model	ω	λ	H_0
$3\lambda H\rho_{\text{de}}$	$-1.088^{+0.0651}_{-0.0448}$	$0.05219^{+0.0349}_{-0.0355}$	$68.35^{+1.47}_{-1.46}$
$3\lambda H\rho_\chi$	$-1.1041^{+0.0467}_{-0.0292}$	$0.0007127^{+0.000256}_{-0.000633}$	$68.91^{+0.875}_{-0.997}$
$3\lambda H(\rho_{\text{de}} + \rho_\chi)$	$-1.105^{+0.0468}_{-0.0288}$	$0.000735^{+0.000254}_{-0.000679}$	$68.88^{+0.854}_{-0.97}$

The mass evaporation rate due to Hawking radiation can be expressed as

$$\frac{dM_{\text{BH}}}{dt} \approx -5.34 \times 10^{25} \left(\sum_i \mathcal{F}_i \right) \left(\frac{M_{\text{BH}}}{\text{g}} \right)^{-2} \text{ g/sec} \quad (3)$$

where, M_{BH} is the mass of black hole and $\sum_i \mathcal{F}_i$ is the sum over all fraction of evaporation, defined as [61],

$$\begin{aligned} \sum_i \mathcal{F}_i = & 1.569 + 0.569 \exp\left(-\frac{0.0234}{T_{\text{BH}}}\right) + 3.414 \exp\left(-\frac{0.066}{T_{\text{BH}}}\right) \\ & + 1.707 \exp\left(-\frac{0.11}{T_{\text{BH}}}\right) + 0.569 \exp\left(-\frac{0.394}{T_{\text{BH}}}\right) \\ & + 1.707 \exp\left(-\frac{0.413}{T_{\text{BH}}}\right) + 1.707 \exp\left(-\frac{1.17}{T_{\text{BH}}}\right) \\ & + 1.707 \exp\left(-\frac{22}{T_{\text{BH}}}\right) + 0.963 \exp\left(-\frac{0.1}{T_{\text{BH}}}\right) \end{aligned} \quad (4)$$

In the above expression, T_{BH} represents the temperature of the black hole given by, $T_{\text{BH}} = 1.05753 \times (M_{\text{BH}}/10^{13}\text{g})^{-1}$. In the case of massive black holes, only the contributions of photon and electron channels are significant. However, in the present work, the mass range of the PBHs are considered to be $\sim 10^{14}$ – 10^{15} g. The temperature of such PBHs are substantially high to radiate in the form of pions, muons, quarks and gluons [20, 62, 63]. As a consequence, besides the γ and electron channels, other channel also contribute remarkably to the IGM heating by producing photons, electrons and positrons via subsequent cascade decay [62, 64, 65]. The energy injection rate per unit volume due to PBHs is given by [20],

$$\left. \frac{dE}{dVdt} \right|_{\text{BH}} = -\frac{dM_{\text{BH}}}{dt} n_{\text{BH}}(z) \quad (5)$$

where, $n_{\text{BH}}(z)$ is the number density of black hole at redshift z . which can be expressed as a function of cosmological redshift (z) and initial mass fraction of primordial black holes (β_{BH}), as,

$$\begin{aligned} n_{\text{BH}}(z) = & \beta_{\text{BH}} \left(\frac{1+z}{1+z_{\text{eq}}} \right)^3 \frac{\rho_{\text{c,eq}}}{\mathcal{M}_{\text{BH}}} \left(\frac{\mathcal{M}_{\text{H,eq}}}{\mathcal{M}_{\text{H}}} \right)^{1/2} \left(\frac{g_\star^i}{g_\star^{\text{eq}}} \right)^{1/12} \\ \approx & 1.46 \times 10^{-4} \beta_{\text{BH}} (1+z)^3 \left(\frac{\mathcal{M}_{\text{BH}}}{\text{g}} \right)^{-3/2} \text{ cm}^{-3}. \end{aligned} \quad (6)$$

IV. TEMPERATURE EVOLUTION

In this Section, the formalism of evolution of baryon temperature (T_b) and the dark matter temperature (T_χ) with redshift z is discussed. As mentioned earlier, we have considered three effects namely DM - baryon scattering, DM - DE interaction and evaporation of PBH in temperature evolution of baryon and dark matter and finally compute the 21-cm brightness temperature (T_{21}). The effect of dark matter - baryon scattering has earlier been addressed in the context of 21-cm signal by [45]. More recently the effect of DM - DE interaction is also included along with DM - baryon scattering by [33]. In the present work, in addition, the effects of PBH evaporation are also included along with DM - baryon scattering and DM - DE interaction in the evolution equations of T_χ and T_b . With all these, the temperature evolution of χ and baryon b can be written as

$$(1+z)\frac{dT_\chi}{dz} = 2T_\chi - \frac{2\dot{Q}_\chi}{3H(z)} - \frac{1}{n_\chi} \frac{2Q}{3H(z)}, \quad (7)$$

$$(1+z)\frac{dT_b}{dz} = 2T_b + \frac{\Gamma_c}{H(z)}(T_b - T_\gamma) - \frac{2\dot{Q}_b}{3H(z)} - \mathcal{J}_{\text{BH}}. \quad (8)$$

where, the last term of Eq. 7 indicates the effects of dark matter - dark energy interaction (see Section II) and the last term of Eq. 8 represents the contribution of PBHs in the form of Hawking radiation [20] given by,

$$\mathcal{J}_{\text{BH}} = \frac{2}{3k_B H(z)} \frac{K_{\text{BH}}}{1 + f_{\text{He}} + x_e}. \quad (9)$$

In Eq. 8, T_γ ($T_\gamma = 2.725(1+z)$ K) is the CMB temperature and Γ_c ($\Gamma_c = \frac{8\sigma_T a_r T_\gamma^4 x_e}{3(1+f_{\text{He}}+x_e)m_e c}$) describes the Compton interaction rate (σ_T and a_r are the Thomson scattering cross-section and radiation constant respectively). The quantities f_{He} and x_e are the fractional abundance of He and ionization fraction respectively. The heating rates \dot{Q}_b and \dot{Q}_χ are estimated as described in [45] (b and χ represent baryon and DM respectively) which depends on the drag term $V_{\chi b}$.

The ionization fraction x_e ($= n_e/n_H$, where n_e and n_H are the number density of free electron and hydrogen respectively) is an important quantity in estimating thermal evolution. It also influences T_b and T_γ simultaneously. This evolution is given by,

$$\frac{dx_e}{dz} = \frac{1}{(1+z)H(z)} [I_{\text{Re}}(z) - I_{\text{Ion}}(z) - I_{\text{BH}}(z)], \quad (10)$$

where $I_{\text{Re}}(z)$ and $I_{\text{Ion}}(z)$ are the standard recombination rate and standard ionization rate respectively. The combined effect of these two coefficients is described as,

$$I_{\text{Re}}(z) - I_{\text{Ion}}(z) = C_P \left(n_H \alpha_B x_e^2 - 4(1-x_e)\beta_B e^{-\frac{3E_0}{4k_B T_\gamma}} \right). \quad (11)$$

In Eq. 11, C_P is the Peebles C factor [66, 67], $E_0 = 13.6$ eV, α_B and β_B are the case B recombination and ionization coefficients respectively.

The expression for α_B (in m^3s^{-1}) as a function of temperature, can be obtained by data fitting as obtained in the work of [68]. The fitted expression of α_B with parameters $a = 4.309$, $b = -0.6166$, $c = 0.6703$, $d = 0.5300$, $F = 1.14$ is given by [29, 68],

$$\alpha_B = 10^{-19} F \left(\frac{at^b}{1 + ct^d} \right), \quad (12)$$

where, t represents the temperature in 10^4K [68–70]. The expression for photoionization coefficient (β_B) (in term of α_B) [29, 70] is,

$$\beta_B = \alpha_B \left(\frac{2\pi\mu_e k_B T_\gamma}{h^2} \right)^{3/2} \exp \left(-\frac{h\nu_{2s}}{k_B T_\gamma} \right), \quad (13)$$

where, μ_e is the reduced mass of electron-proton system and ν_{2s} denotes the frequency for $2s \rightarrow 1s$ transition. The Peebles C factor reads as [67],

$$C_P = \frac{\frac{3}{4}R_{\text{Ly}\alpha} + \frac{1}{4}\Lambda_{2s1s}}{\beta_B + \frac{3}{4}R_{\text{Ly}\alpha} + \frac{1}{4}\Lambda_{2s,1s}}. \quad (14)$$

In the above, $R_{\text{Ly}\alpha}$ represents the rate of escape of Lyman- α ($\text{Ly}\alpha$) photons

$$R_{\text{Ly}\alpha} = 8\pi H / (3n_H(1 - x_e)\lambda_{\text{Ly}\alpha}^3)$$

and $\Lambda_{2s,1s} \approx 8.22\text{s}^{-1}$ [67].

In Eqs. 9 and 10, the parameters K_{BH} and I_{BH} are described as,

$$K_{\text{BH}} = \chi_h f(z) \frac{1}{n_b} \times \frac{dE}{dV dt} \Big|_{\text{BH}}. \quad (15)$$

$$I_{\text{BH}} = \chi_i f(z) \frac{1}{n_b} \frac{1}{E_0} \times \frac{dE}{dV dt} \Big|_{\text{BH}}, \quad (16)$$

where $\chi_i = (1 - x_e)/3$ and $\chi_h = (1 + 2x_e)/3$ are the fraction of the energy deposited in the form of ionization and heating respectively [20, 28, 64, 71, 72]. The factor $f(z)$ is the total fraction of the injected energy deposited into the IGM at redshift z [73–77].

The evolution of relative velocity between the baryonic matter and dark matter ($V_{\chi b} \equiv V_\chi - V_b$) with redshift, as discussed in [45] play an important role in this formalism. This is related to the drag term $D(V_{\chi b})$, between χ and b , as

$$\frac{dV_{\chi b}}{dz} = \frac{V_{\chi b}}{1 + z} + \frac{D(V_{\chi b})}{(1 + z)H(z)}, \quad (17)$$

with initial condition $V_{\chi b} = 29$ km/s. In the above equation, the drag term $D(V_{\chi b})$ is defined as,

$$D(V_{\chi b}) = \frac{d(V_{\chi b})}{dt} = \frac{\rho_m \sigma_0}{m_b + m_\chi} \frac{1}{V_{\chi b}^2} F(r) \quad (18)$$

In Eq. 18, $F(r) = \text{erf}(r/\sqrt{2}) - \sqrt{2/\pi} r e^{-r^2/2}$, where r is defined as $r = V_{\chi b}/u_{\text{th}}$ and $u_{\text{th}} = \sqrt{T_b/m_b + T_\chi/m_\chi}$ is the variance of the thermal relative motion of dark matter - baryon fluid and σ_0 is the dark matter - baryon scattering cross-section while σ_{41} is the same in units of 10^{-41}cm^2 .

V. 21-CM COSMOLOGY

As mentioned earlier, the 21-cm line is originated due to the transition of electrons between the triplet and singlet states of the hydrogen atom (spin 0 and spin 1). The intensity of the 21-cm line is represented by the brightness temperature (T_{21}) which depends on optical depth (τ) and hence the Hubble parameter ($H(z)$). The variation of brightness temperature of the 21-cm hydrogen spectrum with redshift (z) is given by,

$$T_{21} = \frac{T_s - T_\gamma}{1 + z} (1 - e^{-\tau}) \approx \frac{T_s - T_\gamma}{1 + z} \tau, \quad (19)$$

where, T_s and T_γ are spin temperature and CMB temperature respectively at redshift z . As the numerical values of τ for different z are very small, we use the approximation in the above equation (Eq. 19). The optical depth (τ) is given by,

$$\tau = \frac{3}{32\pi} \frac{T_\star}{T_s} n_{\text{HI}} \lambda_{21}^3 \frac{A_{10}}{H(z) + (1 + z)\delta_r v_r} \quad (20)$$

where, λ_{21} (≈ 21 cm) is the 21-cm wavelength, T_\star ($= hc/k_B \lambda_{21} = 0.068$ K) is the 21-cm temperature, A_{10} ($= 2.85 \times 10^{-15} \text{s}^{-1}$) is the Einstein coefficient [78] and $\delta_r v_r$ represents the peculiar velocity gradient.

The spin temperature T_s describes the ratio n_1/n_0 , where n_1 and n_0 are excited state and ground state neutral hydrogen number densities respectively, given by $n_1/n_0 = 3 \exp(-T_\star/T_s)$. In equilibrium T_s is given by

$$T_s = \frac{T_\gamma + y_c T_b + y_{\text{Ly}\alpha} T_{\text{Ly}\alpha}}{1 + y_c + y_{\text{Ly}\alpha}}, \quad (21)$$

where, $y_{\text{Ly}\alpha}$ represents the Wouthuysen-Field effect in T_s . The quantities y_c , and $T_{\text{Ly}\alpha}$ are the collisional coupling parameters and the Lyman- α background temperature respectively [19] whereas y_c and $y_{\text{Ly}\alpha}$ are defined as $y_c = \frac{C_{10} T_\star}{A_{10} T_b}$ and $y_{\text{Ly}\alpha} = \frac{P_{10} T_\star}{A_{10} T_{\text{Ly}\alpha}} e^{0.3 \times (1+z)^{1/2} T_b^{-2/3} \left(1 + \frac{0.4}{T_b}\right)^{-1}}$ [20, 79–81]. C_{10} is the collision deexcitation rate of the hyperfine level and $P_{10} \approx 1.3 \times 10^{-21} S_\alpha J_{-21} \text{s}^{-1}$ is the

deexcitation rate due to Lyman- α , where S_α and J_{-21} are the spectral distraction factor [82] and the Lyman- α background intensity respectively. The background intensity J_{-21} is estimated as described in [83].

It is to be noted that the effects of the Lyman- α photons from the first stars, play a significant role for the shape of the spin temperature curve when $z \lesssim 25$. In the epoch of the cosmic dark age, the CMB photons contribute to flip the spin state of hydrogen atoms. As a consequence, the spin temperature (T_s) gets closer to the CMB temperature (over inverse of the redshift). However, later ($z \lesssim 25$), the Lyman- α photons from the new-born stars lead to quick transition of the spin temperature $T_s = T_b$. As a result, the spin temperature becomes almost equal to the baryon temperature during the age of cosmic dawn [84, 85] (Fig. 1). This phenomenon is known as the Wouthuysen-Field effect. The strength of the Wouthuysen-Field effect depends on the rate of scattering of the Lyman- α photons in the IGM [86].

VI. CALCULATIONS AND RESULTS

In this work, we explore the 21-cm anomalous hydrogen absorption line in reionization era by considering the possible simultaneous effects of Hawking radiation from PBHs along with the DM - baryon interaction. In doing this, we numerically solve seven coupled equations, (Eqs. 1, 2, 3, 7, 8, 10 and 17) simultaneously. The evolution is initiated at redshift $z = 1010$ as described in the work of Muñoz [45], when the baryons are assumed to be tightly coupled with the CMB photons (i.e. $T_b \cong T_\chi$). At $z = 1010$, the initial relative velocity is considered to be ~ 29 km/s and the temperature of DM fluid is assumed to be $T_\chi = 0$. It is to be mentioned that, even if a slightly warm dark matter candidate is taken into account, the evolution remains almost the same (it has also been discussed by Muñoz [45]). Since we consider two matter fluids (dark matter fluid and baryon fluid) in this system, the cooler fluid (dark matter fluid) tends to heat up at the expense of the temperature of the comparatively warmer fluid (baryon fluid) as an outcome of the temperature exchange between them (even without IDE effect (Fig. 4)). Although this heating rate is essentially proportional to $(T_b - T_\chi)$, the heating rate gets perturbed in presence of the drag term ($V_{\chi b}$). A detailed analysis regarding this thermal effect has been addressed in [45]. In Fig. 1, the evolution of baryon temperature (T_b), CMB temperature (T_γ) and the corresponding spin temperature (T_s) are plotted as a function of redshift z . The solid red line in Fig. 1 describes the baryon temperature (T_b). Spin temperature (T_s , red dashed line) variations in presence of PBHs of mass $\mathcal{M}_{\text{BH}} = 10^{14}$ g and dark matter mass $m_\chi = 1$ GeV, with the IDE Model I (model

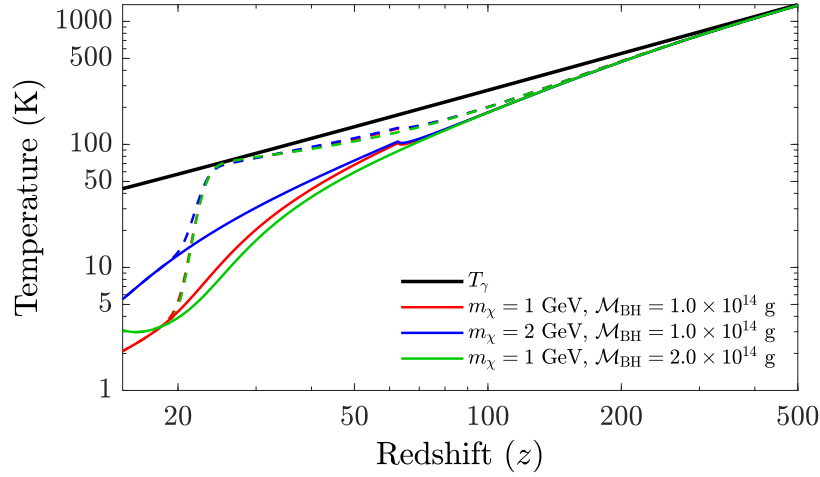


FIG. 1. The variation of baryon temperature T_b , background temperature T_γ , spin temperature T_s with redshift z . The black solid line represents the variation of T_γ and the coloured solid lines and coloured dashed lines correspond to the variations of T_b and T_s respectively with z , for different sets of dark matter mass m_χ and PBH mass \mathcal{M}_{BH} . Note that for T_s , the plots for all three sets almost coincide. For both T_b and T_s , the computations are made with Model I (Table I and II) only.

parameters are chosen from Table. II) is also shown. The blue and green solid and dashed lines are for the same with $m_\chi = 2 \text{ GeV}$, $\mathcal{M}_{\text{BH}} = 1.0 \times 10^{14} \text{ g}$ and $m_\chi = 1 \text{ GeV}$, $\mathcal{M}_{\text{BH}} = 2.0 \times 10^{14} \text{ g}$ respectively. In all the cases however Model I for DM - DE interaction is used. It can also be seen that, while the variation of T_b with z differ for different choices of m_χ and \mathcal{M}_{BH} below $z \sim 100$. Such variations for T_s are barely observed except very mildly around $z \sim 20$.

In Fig. 2 we demonstrate how the 21-cm brightness temperature T_{21} is affected for different dark matter masses m_χ and various dark matter - baryon scattering cross-sections (different values of σ_{41}). We plot in Fig. 2 the variations of T_{21} with z for different values of m_χ for a fixed value of $\sigma_{41} = 1$ (Fig. 2a) and for different values of σ_{41} for a fixed value of $m_\chi = 1 \text{ GeV}$ (Fig. 2b). For both the cases, the PBH mass is fixed at $\mathcal{M}_{\text{BH}} = 1.5 \times 10^{14} \text{ g}$. It is to be noted that, both Fig. 2a and Fig. 2b show the variation of T_{21} at higher redshift era ($\gtrsim 50$).

In presence of the DM - DE interaction, the dark matter and dark energy density parameters evolve non-linearly with redshift z . As a consequence, remarkable variations in the evolution of Hubble parameter H are obtained (see Fig. 3). In Fig. 3, the variation of Hubble parameter as

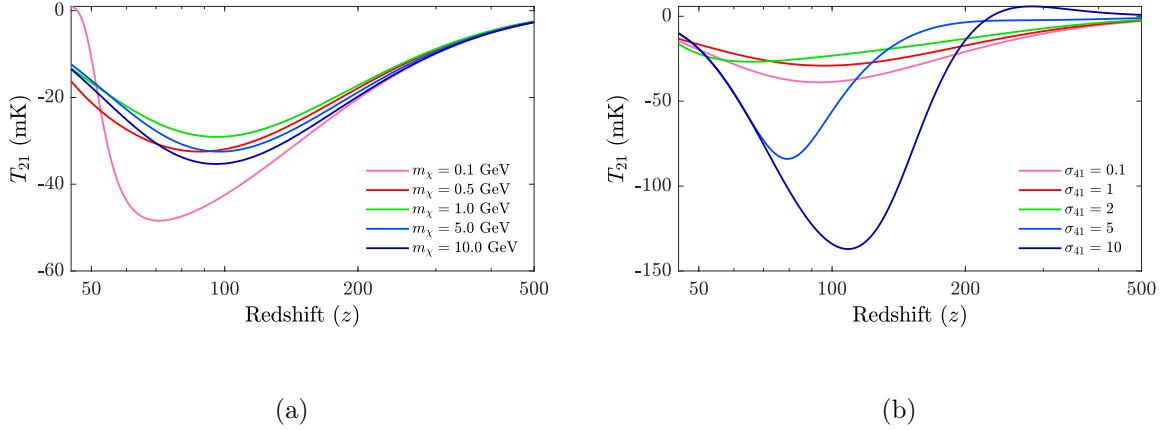


FIG. 2. Variations of brightness temperature (T_{21}) with redshift (z) (a) for different values of m_χ (0.1 GeV, 0.5 GeV, 1 GeV, 5 GeV and 10 GeV) in presence of PBH mass $\mathcal{M}_{\text{BH}} = 1.5 \times 10^{14}$ g and $\sigma_{41} = 1$. Fig. 2(b) (right panel) describes the variations of T_{21} for different values of σ_{41} ($\sigma_{41} = 0.1, 1, 2, 5, 10$) when the PBH mass $\mathcal{M}_{\text{BH}} = 10^{14}$ g and dark matter mass $m_\chi = 1$ GeV are chosen.

a dimensionless quantity $H(z)/H_0$ (H_0 is the current value of Hubble parameter) is shown with redshift z . The left panel of Fig. 3 (Fig. 3a, 3c and 3e) shows the variation of Hubble parameter with redshift z for different values of IDE coupling parameter λ , where the different values of λ are represented by different colours (cyan to magenta, (see colour-bars)). On the other hand, Figs. 3b, 3d and 3f (right panel of Fig. 3) show the variations of $H(z)/H_0$ with λ and the equation of state parameter (ω) simultaneously. The plots Fig. 3a, 3c and 3e (left panel of Fig. 3) correspond to Model I, II and III (Tables I, II) respectively of DM - DE interaction. In the right panel of Fig. 3, the plots of Fig. 3b, 3d and 3f also correspond to Model I, II and III respectively. In all the three plots of the left panel of Fig. 3 (for Models I, II and III), the values of the DE equation of state parameter ω for the corresponding models are adopted from Table II. In each of the plots of Fig. 3, the dashed black line represents the Λ CDM case ($\lambda = 0$). Analysing all the plots in Fig. 3, one can conclude that, the evolution of Hubble parameter is almost identical in the case of Model II and Model III where the variations mostly depend on λ (see Fig. 3d and 3e, the dependence on ω is minimal) and the variation is almost linear in nature (see Fig. 3c and 3d). Nonetheless, very small difference can be observed between Model II and Model III in Fig. 3d and 3e (also comparing Fig. 3c and 3d). In contrast, in case of Model I, both the parameters, λ and ω , are equally significant in the Hubble parameter evolution (see Fig. 3b). From Fig. 3a, it can be observed that, initially $H(z)/H_0$ decreases gradually with increasing coupling parameter λ . But later (for higher values

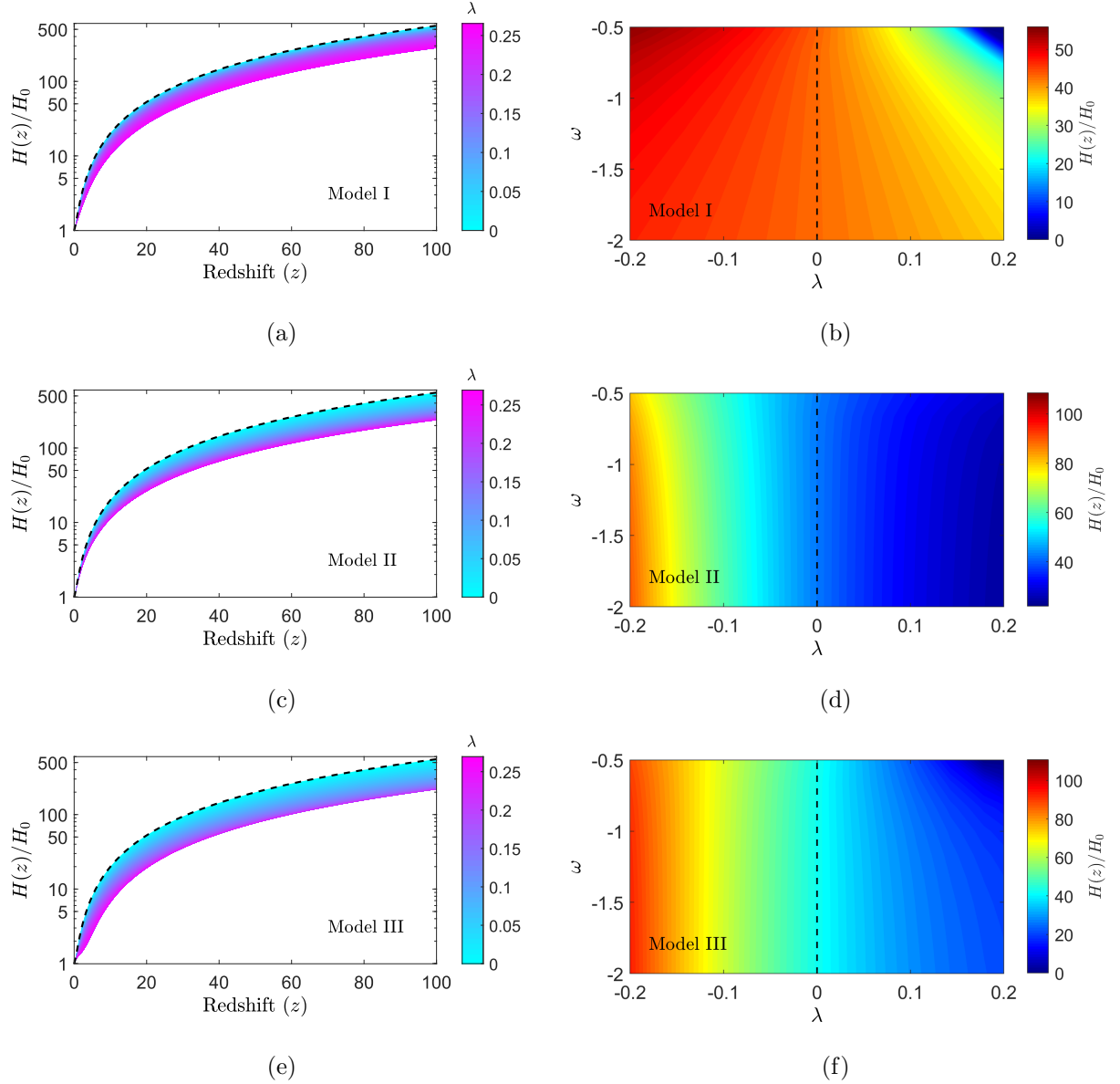


FIG. 3. Evolution of Hubble parameter ($H(z)$) for different IDE models (Model I, Model II and Model III) with different values of coupling parameters λ . The plots on the left panel (Fig. 3a, 3c and 3e) give the $H(z)$ evolution for different values of λ where the other parameters (ω and H_0) are chosen from Table II. The plots on right panel (Fig. 3b, Fig. 3d and Fig. 3f) show the variation of $H(z)$ with simultaneous variations of the parameters λ and ω (keeping H_0 fixed) at redshift $z = 17.2$. The black dashed line represents the variations of $H(z)$ for the Λ CDM case in each figure.

of λ) $H(z)/H_0$ suffers rapid fall with increasing λ . Therefore, although the allowed range of λ for Model I is $\lambda < -2\omega\Omega_\chi$ (see Table I), we limit this range to $0 < \lambda < 0.25$ for the current work.

Incorporating the above mentioned modifications in the density parameters and hence the Hubble parameter, the temperature evolution of the Universe is addressed in presence of the PBH and

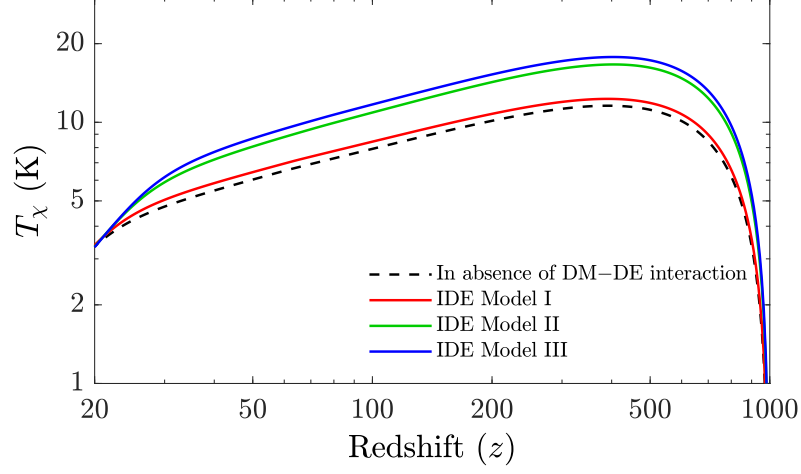


FIG. 4. Variation of dark matter temperature (T_χ) with redshift z for different IDE models. For all these plots we consider $\lambda = 0.05$, $\mathcal{M}_{\text{BH}} = 10^{14} \text{g}$, $\beta_{\text{BH}} = 10^{-29}$, $m_\chi = 1 \text{ GeV}$, $\sigma_{41} = 1$, while ω is taken from Table II for different IDE models.

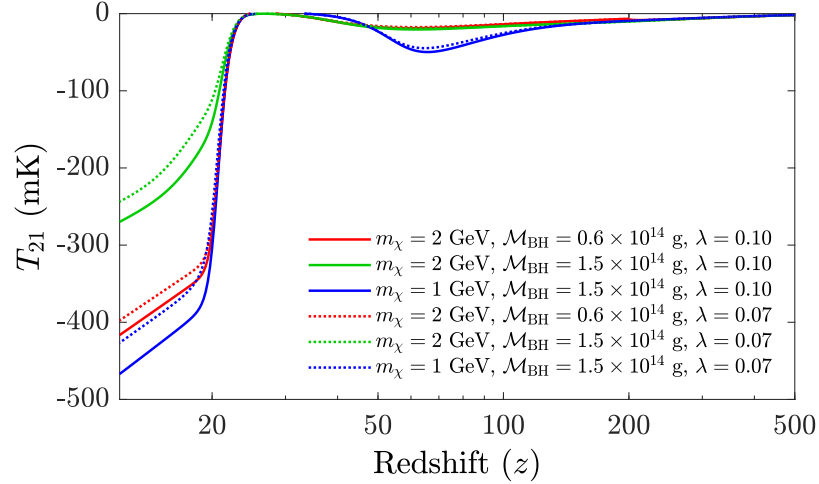


FIG. 5. Brightness temperature (T_{21}) vs redshift (z) graph for different values of DM mass (m_χ), PBH mass (\mathcal{M}_{BH}) and IDE coupling parameter λ for Model I.

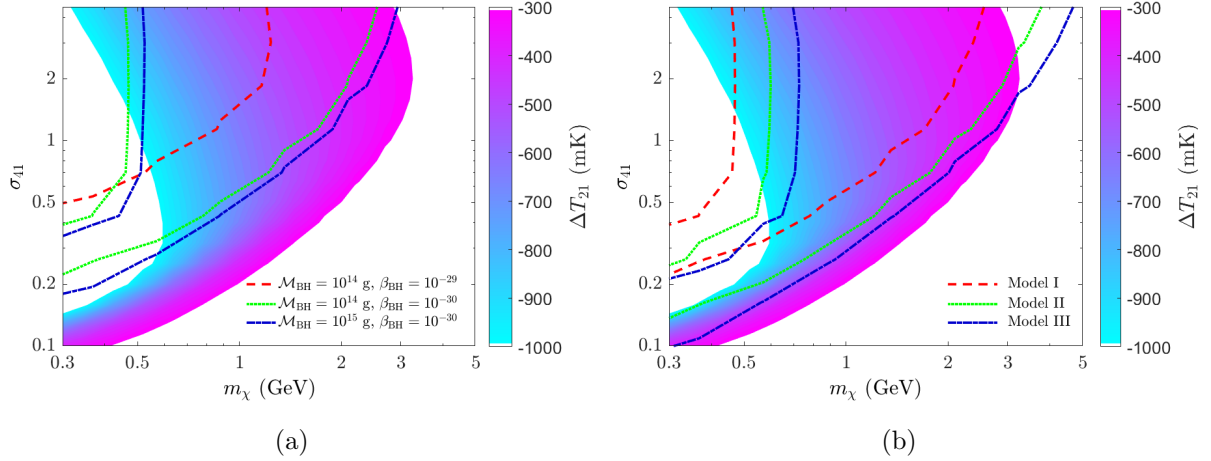


FIG. 6. The allowed region of the 21-cm brightness temperature in $m_\chi - \sigma_{41}$ space. The coloured shaded region represents the allowed region for the case of Λ CDM model in both the cases. In this coloured region, DM - DE interaction has not been considered. The coloured lines represent the similar bounds for different values of PBH parameters in Fig. 6a, for the case of Model I whereas, in Fig. 6b, the estimated bounds are shown for different IDE models (with $\mathcal{M}_{\text{BH}} = 10^{14}$ g, $\beta_{\text{BH}} = 10^{-30}$ and $\lambda = 0.1$)

the dark matter - baryon interaction (scattering). The effect of DM-DE interaction is manifested in the evolution of dark matter temperature (T_χ). In Fig. 4, the variation of T_χ with z is shown for different IDE models and compared with the same in absence of the interaction between two dark sector components of the Universe (i.e. dark matter and dark energy). All the plots in Fig. 4 are computed for $\lambda = 0.05$, $\mathcal{M}_{\text{BH}} = 10^{14}$ g, $\beta_{\text{BH}} = 10^{-29}$, $m_\chi = 1$ GeV, $\sigma_{41} = 1$, the values of ω for different IDE models are taken from Table II. From Fig. 4 it can be seen that, T_χ increases as a outcomes of the interactions between dark matter and dark energy. This phenomenon indicates that, a significant amount of energy transfers from dark energy to the dark matter, due to DM-DE interaction. It is also noticed that the amount of energy transfer is remarkably high for the case of IDE Model II and IDE model III in comparison to the Model I. In Fig. 5, we plot the 21-cm brightness temperatures (T_{21}) for different values of IDE coupling parameter ($\lambda = 0.07$ and 0.10) for dark matter masses $m_\chi = 2$ GeV and 1 GeV and PBH masses $\mathcal{M}_{\text{BH}} = 0.6 \times 10^{14}$ g and 0.6×10^{14} g while keeping β_{BH} and σ_{41} fixed at 10^{-29} and 3 respectively in the case of IDE Model I. From this figure (Fig. 5), it can be noticed that, besides DM mass and PBH mass, IDE coupling parameter λ also modifies the brightness temperature remarkably. A detail study for the variation due to σ_{41} has been carried out in Fig. 6.

The allowed ranges of the dark matter mass m_χ and σ_{41} , that satisfy the EDGES result for T_{21} are also estimated. The allowed regions in $m_\chi - \sigma_{41}$ parameter space are shown in Fig. 6 for

different PBH masses (Fig. 6a) and also for three different IDE models (Fig. 6b). The contour plots are generated for a fixed value of $z = 17.2$. In what follows the brightness temperature at $z = 17.2$ is represented by ΔT_{21} unless otherwise mentioned. The EDGES limit of the brightness temperature (T_{21}) at $z \sim 17.2$ lie within the range of $-300 \text{ mK} \geq T_{21} \geq -1000 \text{ mK}$. In the current analysis, we estimate the limit for m_χ and σ_{41} using the above mentioned constraint ($-300 \text{ mK} \geq T_{21} \geq -1000 \text{ mK}$). In Fig. 6a, the calculated allowed zones in the $m_\chi - \sigma_{41}$ plane are plotted for Λ CDM model using the colour code (coloured shaded region), where the individual colours within the coloured shaded region indicate the different values of ΔT_{21} (colour code is described in the corresponding colour-bar). This may be mentioned that the limits on m_χ obtained from these contour plots agree with a similar calculation given in [46] (i.e. $m_\chi \leq 3 \text{ GeV}$). In both the plots (a) and (b) of Fig. 6, the coloured contour plots are generated by varying m_χ and σ_{41} and computing ΔT_{21} . For the coloured shaded regions (not the line contours) in both Fig. 6a and 6b, only the dark matter - baryon interaction is considered and the relevant coupled differential parameters are simultaneously solved numerically. The other contour plots generated using all the effects considered here namely, the DM - baryon interaction, DM - DE interaction and PBH evaporations are shown by line contour plots (allowed region enclosed by lines) in both Fig. 6a and Fig. 6b. In these latter cases the allowed regions are bound by different pairs of lines in $m_\chi - \sigma_{41}$ plane. In Fig. 6a, three different line contours are for three different sets of values of PBH masses and β_{BH} when Model I (Table I and II) is used for DM - DE interaction in all the three line contour plots. In Fig. 6b, the three allowed contours (area enclosed by different lines) in $m_\chi - \sigma_{41}$ plane are generated with three IDE models (Model I, II and III, Table I, II) while the PBH mass and β_{BH} are kept fixed at values of 10^{14} g and 10^{-29} respectively. From Fig. 6a it can be seen that the region enclosed by red dashed line corresponds to the $m_\chi - \sigma_{41}$ allowed region when PBH mass $\mathcal{M}_{\text{BH}} = 10^{14} \text{ g}$ and $\beta_{\text{BH}} = 10^{-29}$ are chosen with Model I for DM - DE interaction. Similarly, the region enclosed by the green dotted lines specifies the allowed region when $\mathcal{M}_{\text{BH}} = 10^{15} \text{ g}$, $\beta_{\text{BH}} = 10^{-30}$ are considered. From Fig. 6a this can be observed that as \mathcal{M}_{BH} decreases (Hawking radiation increases) the allowed region shifts towards higher σ_{41} and lower m_χ region. A similar trend is also observed for the IDE Model I (Fig. 6b). On the other hand, in the case of IDE Model II and III, the allowed region shifts toward higher values of m_χ .

Finally, a detailed study has been carried out to explore similar bounds in the $\mathcal{M}_{\text{BH}} - \lambda$ plane for individual IDE models and its variation with m_χ as well. We use three different values of dark matter masses namely $m_\chi = 0.5 \text{ GeV}$, 1.0 GeV and 1.5 GeV . In each of these cases, the value of σ_{41} is set to 1.0. These are shown in Fig. 7. The first, second and third row correspond to

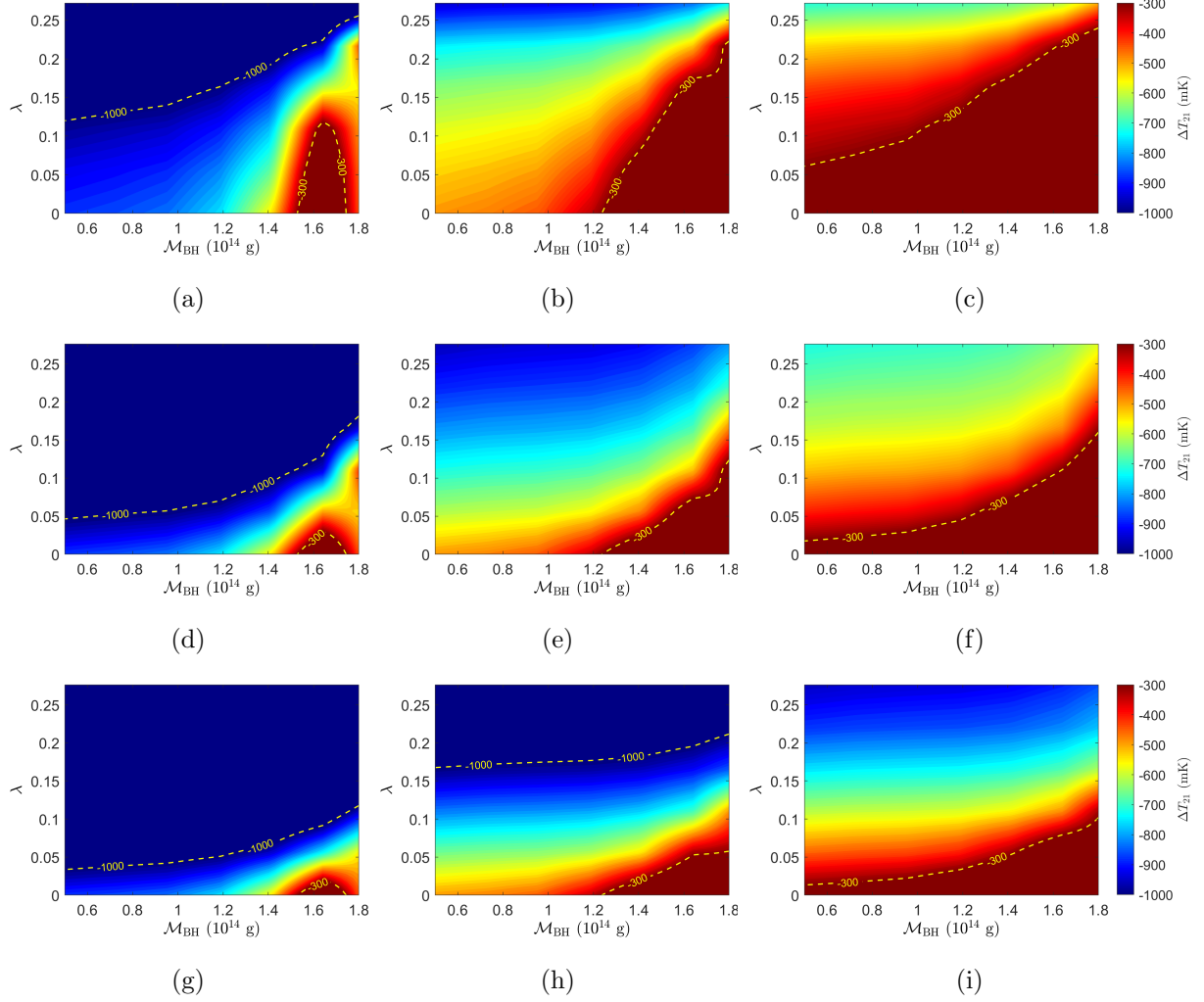


FIG. 7. Variation of ΔT_{21} with PBH mass and DE-DM coupling parameter λ for different DM masses and IDE models (see text for details).

the IDE Model I, II and III respectively while the plots in each of the columns 1, 2 and 3 are for three fixed dark masses, $m_\chi = 0.5$ GeV, 1 GeV, 1.5 GeV respectively. For example, Fig. 7a shows the fluctuation of ΔT_{21} in $\mathcal{M}_{\text{BH}} - \lambda$ space for $m_\chi = 0.5$ GeV and the IDE Model I, where the value of ΔT_{21} at each point is described in the colour bar shown at the end of each row. In all the plots of Fig. 7, the yellow dashed lines represent the bounds from EDGES result. Fig. 7b and Fig. 7c describe the same for $m_\chi = 1.0$ GeV and 1.5 GeV respectively for IDE Model I. From these figures it can be seen that, as \mathcal{M}_{BH} increases, ΔT_{21} increases for a fixed value of λ (except a little distortion at $\mathcal{M}_{\text{BH}} = 1.7 \times 10^{14} \text{g}$). It can also be noticed (from Fig. 7a, 7b and 7c) that as m_χ increases (from column 1 to column 3), ΔT_{21} also increases. As mentioned, results for Model II and Model III are furnished in plots 7d, 7e, 7f and in plots 7g, 7h, 7i respectively. From these figures

(all plots of Fig. 7), it can be noticed that, when $m_\chi = 0.5$ GeV, λ values for each of the three IDE model constraints (see benchmark points described in Table II) satisfy the EDGES limits for $\mathcal{M}_{\text{BH}} \lesssim 1.5 \times 10^{14}$ g and $\mathcal{M}_{\text{BH}} \gtrsim 1.8 \times 10^{14}$ g. Those constraints also agree with the EDGES limit for $\mathcal{M}_{\text{BH}} \lesssim 1.2 \times 10^{14}$ g, when $m_\chi = 1.0$ is considered. But, for higher values of m_χ ($m_\chi = 1.5$ GeV), the benchmark values of λ does not satisfy the EDGES limit of ΔT_{21} (see Fig. 6c, Fig. 6f and Fig. 6i).

VII. SUMMARY AND DISCUSSIONS

In this work, the effect of PBH evaporation on 21-cm EDGES signal is principally addressed while taking into consideration other important effects arising out of dark matter scattering on baryons and also dark matter-dark energy interactions that can possibly influence the observed temperature of 21-cm signal during reionization epoch. The PBHs can inject energy into the system through their evaporation through Hawking radiation. In addition the dark matter scattering off baryons also transfers heat to or from the system depending on the mass of dark matter. Also, the interactions between dark matter and dark energy can also influence the 21-cm brightness temperature. To this end three such interacting dark energy (IDE) models are adopted where non-minimal coupling of two dark sectors namely dark matter and dark energy is adopted and the energy transfer due to the IDE and dark matter-baryon scattering are properly incorporated in the relevant evolution equations for baryon temperature, dark matter temperature etc.

The energy injection rate for the PBH evaporations or in other words the contribution of PBHs in the form of Hawking radiation is included in the present work for the computation of evolution of baryon temperature. In fact a set of coupled differential equations involving evolutions of baryon temperature, dark matter temperature, the background temperature, ionization fraction, dark matter baryon relative velocity (leading to the drag term) etc. are solved computationally to obtain the baryon temperature, spin temperature, the optical depth etc. to finally compute the 21-cm temperature T_{21} . It is to be noted that in the present calculations for spin temperature T_s , the effect of Lyman- α background is also included where Wouthuysen-Field effect is important.

The effect of PBH on the 21-cm brightness temperature is demonstrated in the present work for different PBH masses ($\sim 10^{14} - 10^{15}$ gm) and initial PBH mass fraction β_{BH} (related to black hole number density n_{BH}). For the reported 21-cm EDGES signal, the allowed regions in the parameter space of dark matter mass and dark matter - baryon scattering cross-sections ($m_\chi - \sigma$) for different IDE models (adopted in this work) are obtained for various PBH masses \mathcal{M}_{BH} and β_{BH} . It is seen

that heavier PBH masses appear to favour region of higher m_χ and lower σ_{41} .

It is also to be noted that when dark matter-dark energy interactions are considered, the dark matter density ρ_χ and dark energy density ρ_{DE} do not evolve as $\sim (1+z)^3$ and $(1+z)^{3(1+\omega)}$ suggested by standard cosmology. Therefore the evolution of expansion rate of the Universe ($H(z)$) is modified due to dark matter-dark energy interactions which in turn affects the optical depth and spin temperature of the 21-cm transition. The evolution of Hubble parameter is also computed in detail in the present work for all the three IDE models adopted.

The dark matter-dark energy interaction parameter λ has been probed in this work along with the effects of PBH. The upper and lower limits of the IDE parameter λ for three IDE models (adopted in this work) have been investigated for different PBH masses (within the ball park of 10^{14} gm) for the range of T_{21} given by the EDGES experiment at reionization era. This appears that the model constraints described in Table II satisfy the EDGES limit for relatively lower masses of dark matter (≤ 1.0 GeV). It can be observed from Fig. 4 that, although the natures of the evolution of dark matter temperature with z are similar for all the IDE Models I, II and III as also for the case of no DM-DE interaction in the redshift region $1000 \leq z \lesssim 30$, the temperature T_χ for IDE Models I and II always lie above the T_χ for Model I and for no DM-DE interaction case. From Fig. 4 it can be seen that, in case of $m_\chi \sim \text{GeV}$, the maximum fluctuation in T_χ is ~ 5 K for different IDE models. Although a very tiny fluctuation appears in the temperature of dark matter fluid due to DM-DE interaction, it may seed a significant contribution in the global structure formation [87]. From Fig. 7, the limit of IDE coupling parameter λ for IDE Model I, II and III can be observed. It can be seen that, although the limits of λ barely satisfy EDGES's limit for $m_\chi = 0.5$ GeV and 1.0 GeV for all three IDE models, they do not agree with the EDGES's limit for higher masses of dark matter particles ($m_\chi = 1.5$ GeV). Models II and III are very tightly constrained by low- ℓ CMB spectrum. The dark matter mass of $m_\chi \sim 0.5$ GeV, 1 GeV are well within the limit of structure formation. Future results related to 21-cm physics from early Universe would throw more light to all these issues and the thermal evolution and dynamics of the early Universe.

ACKNOWLEDGEMENTS

One of the authors (A.H.) wishes to acknowledge the support received from St. Xavier's College, Kolkata and the University Grant Commission (UGC) of the Government of India, for providing financial support, in the form of UGC-CSIR NET-JRF. One of the authors (MP) thanks the DST-

INSPIRE fellowship (DST/INSPIRE/FELLOWSHIP/IF160004) grant by DST, Govt. of India.

- [1] J.D. Bowman, A.E.E. Rogers, R.A. Monsalve, T.J. Mozdzen and N. Mahesh, *Nature* **555** (2018) 67.
- [2] M.Y. Khlopov, *Res. Astron. Astrophys.* **10** (2010) 495.
- [3] K.M. Belotsky, A.E. Dmitriev, E.A. Esipova, V.A. Gani, A.V. Grobov, M.Y. Khlopov et al., *Mod. Phys. Lett. A* **29** (2014) 1440005.
- [4] K.M. Belotsky, V.I. Dokuchaev, Y.N. Eroshenko, E.A. Esipova, M.Y. Khlopov, L.A. Khromykh et al., *Eur. Phys. J. C* **79** (2019) 246.
- [5] J. García-Bellido, *Journal of Physics: Conference Series* **840** (2017) 012032.
- [6] P. Ivanov, P. Naselsky and I. Novikov, *Phys. Rev. D* **50** (1994) 7173.
- [7] B.J. Carr and J.E. Lidsey, *Phys. Rev. D* **48** (1993) 543.
- [8] B.J. Carr, J.H. Gilbert and J.E. Lidsey, *Phys. Rev. D* **50** (1994) 4853.
- [9] J. García-Bellido, A. Linde and D. Wands, *Phys. Rev. D* **54** (1996) 6040.
- [10] A. Taruya, *Phys. Rev. D* **59** (1999) 103505.
- [11] S. Pi, Y. li Zhang, Q.-G. Huang and M. Sasaki, *JCAP* **2018** (2018) 042.
- [12] B.A. Bassett and S. Tsujikawa, *Phys. Rev. D* **63** (2001) 123503.
- [13] E. Cotner and A. Kusenko, *Phys. Rev. Lett.* **119** (2017) 031103.
- [14] E. Cotner, A. Kusenko and V. Takhistov, *Phys. Rev. D* **98** (2018) 083513.
- [15] E. Cotner and A. Kusenko, *Phys. Rev. D* **96** (2017) 103002.
- [16] C.J. Hogan, *Phys. Lett. B* **143** (1984) 87 .
- [17] A. Polnarev and R. Zembowicz, *Phys. Rev. D* **43** (1991) 1106.
- [18] K. ichi Maeda, K. Sato, M. Sasaki and H. Kodama, *Phys. Lett. B* **108** (1982) 98 .
- [19] S.J. Clark, B. Dutta, Y. Gao, Y.-Z. Ma and L.E. Strigari, *Phys. Rev. D* **98** (2018) 043006.
- [20] Y. Yang, *Phys. Rev. D* **102** (2020) 083538.
- [21] A.A. Costa, R.C.G. Landim, B. Wang and E. Abdalla, *Eur. Phys. J. C* **78** (2018) .
- [22] Y. Wang and G.-B. Zhao, *Astrophys. J.* **869** (2018) 26.
- [23] C. Li and Y.-F. Cai, *Phys. Lett. B* **788** (2019) 70–75.
- [24] X. Xu, Y.-Z. Ma and A. Weltman, *Phys. Rev. D* **97** (2018) .
- [25] S. Kumar and R.C. Nunes, *Phys. Rev. D* **96** (2017) .
- [26] S. Kumar, R.C. Nunes and S.K. Yadav, *Eur. Phys. J. C* **79** (2019) .
- [27] O. Mena, S. Palomares-Ruiz, P. Villanueva-Domingo and S.J. Witte, *Phys. Rev. D* **100** (2019) 043540.
- [28] K.J. Mack and D.H. Wesley, *Primordial black holes in the dark ages: Observational prospects for future 21cm surveys*, 2008.
- [29] K.L. Pandey and A. Mangalam, *J. Astrophys. Astro.* **39** (2018) 9.

- [30] A. Hektor, G. Hütsi, L. Marzola, M. Raidal, V. Vaskonen and H. Veermäe, *Phys. Rev. D* **98** (2018) 023503.
- [31] H. Tashiro and N. Sugiyama, *Mon. Not. Roy. Astron. Soc.* **435** (2013) 3001.
- [32] C. Li, X. Ren, M. Khurshudyan and Y.-F. Cai, *Phys. Lett. B* **801** (2020) 135141.
- [33] U. Mukhopadhyay, D. Majumdar and K.K. Datta, *Phys. Rev. D* **103** (2021) 063510.
- [34] B. Wang, E. Abdalla, F. Atrio-Barandela and D. Pavón, *Rep. Prog. Phys.* **79** (2016) 096901.
- [35] E. Di Valentino, A. Melchiorri and O. Mena, *Phys. Rev. D* **96** (2017) 043503.
- [36] G.R. Farrar and P.J.E. Peebles, *Astrophys. J.* **604** (2004) 1–11.
- [37] M.R. Buckley and P.J. Fox, *Phys. Rev. D* **81** (2010) .
- [38] B. Holdom, *Phys. Lett. B* **166** (1986) 196.
- [39] E.J. Chun, J.-C. Park and S. Scopel, *JHEP* **2011** (2011) .
- [40] C. Dvorkin, T. Lin and K. Schutz, *Cosmology of sub-mev dark matter freeze-in*, Sep, 2021. 10.1103/physrevlett.127.111301.
- [41] E.O. Nadler, V. Gluscevic, K.K. Boddy and R.H. Wechsler, *Astrophys. J.* **878** (2019) L32.
- [42] A. Bhoonah, J. Bramante, F. Elahi and S. Schon, *Phys. Rev. Lett.* **121** (2018) .
- [43] E.D. Kovetz, V. Poulin, V. Gluscevic, K.K. Boddy, R. Barkana and M. Kamionkowski, *Phys. Rev. D* **98** (2018) .
- [44] G.D. Mack, J.F. Beacom and G. Bertone, *Phys. Rev. D* **76** (2007) .
- [45] J.B. Muñoz, E.D. Kovetz and Y. Ali-Haïmoud, *Phys. Rev. D* **92** (2015) 083528.
- [46] R. Barkana, *Nature* **555** (2018) 71.
- [47] E. Aprile, J. Aalbers, F. Agostini, M. Alfonsi, L. Althueser, F. Amaro et al., *Phys. Rev. Lett.* **121** (2018) .
- [48] D. Akerib, S. Alsum, H. Araújo, X. Bai, A. Bailey, J. Balajthy et al., *Phys. Rev. Lett.* **118** (2017) .
- [49] X. Cui, A. Abdukerim, W. Chen, X. Chen, Y. Chen, B. Dong et al., *Phys. Rev. Lett.* **119** (2017) .
- [50] M.S. Mahdawi and G.R. Farrar, *JCAP* **2018** (2018) 007–007.
- [51] Z.-K. Guo, N. Ohta and S. Tsujikawa, *Phys. Rev. D* **76** (2007) 023508.
- [52] E. Di Valentino, A. Melchiorri, O. Mena and S. Vagnozzi, *Phys. Rev. D* **101** (2020) 063502.
- [53] A.A. Costa, X.-D. Xu, B. Wang and E. Abdalla, *JCAP* **2017** (2017) 028.
- [54] O. Bertolami, F. Gil Pedro and M. Le Delliou, *Phys. Lett. B* **654** (2007) 165 .
- [55] J.-H. He, B. Wang and E. Abdalla, *Phys. Rev. D* **83** (2011) 063515.
- [56] L. Santos, W. Zhao, E.G.M. Ferreira and J. Quintin, *Phys. Rev. D* **96** (2017) 103529.
- [57] W. Yang, S. Pan and A. Paliathanasis, *Mon. Not. Roy. Astron. Soc.* **482** (2018) 1007.
- [58] M. Le Delliou, R.J.F. Marcondes and G.B. Lima Neto, *Mon. Not. Roy. Astron. Soc.* **490** (2019) 1944.
- [59] M. Gavela, D. Hernández, L.L. Honorez, O. Mena and S. Rigolin, *JCAP* **2009** (2009) 034.
- [60] J.-H. He, B. Wang and E. Abdalla, *Phys. Lett. B* **671** (2009) 139 .
- [61] J.H. MacGibbon, *Phys. Rev. D* **44** (1991) 376.
- [62] J.H. MacGibbon and B.R. Webber, *Phys. Rev. D* **41** (1990) 3052.

- [63] B.J. Carr, K. Kohri, Y. Sendouda and J. Yokoyama, *Phys. Rev. D* **94** (2016) 044029.
- [64] X. Chen and M. Kamionkowski, *Phys. Rev. D* **70** (2004) 043502.
- [65] B.J. Carr, K. Kohri, Y. Sendouda and J. Yokoyama, *Phys. Rev. D* **81** (2010) 104019.
- [66] P.J.E. Peebles, *Astrophys. J.* **153** (1968) 1.
- [67] Y. Ali-Haïmoud and C.M. Hirata, *Phys. Rev. D* **83** (2011) 043513.
- [68] D. Pequignot, P. Petitjean and C. Boisson, *Astron. Astrophys.* **251** (1991) 680.
- [69] D.G. Hummer, *Mon. Not. Roy. Astron. Soc.* **268** (1994) 109.
- [70] S. Seager, D.D. Sasselov and D. Scott, *Astrophys. J.* **523** (1999) L1.
- [71] L. Zhang, X. Chen, M. Kamionkowski, Z.-G. Si and Z. Zheng, *Phys. Rev. D* **76** (2007) 061301(R).
- [72] S.R. Furlanetto, S.P. Oh and E. Pierpaoli, *Phys. Rev. D* **74** (2006) 103502.
- [73] S. Galli, T.R. Slatyer, M. Valdes and F. Iocco, *Phys. Rev. D* **88** (2013) 063502.
- [74] M.S. Madhavacheril, N. Sehgal and T.R. Slatyer, *Phys. Rev. D* **89** (2014) 103508.
- [75] T.R. Slatyer, *Phys. Rev. D* **93** (2016) 023521.
- [76] H. Liu, G.W. Ridgway and T.R. Slatyer, *Phys. Rev. D* **101** (2020) 023530.
- [77] S.K. Acharya and R. Khatri, *JCAP* **06** (2020) 018.
- [78] Y. Ali-Haïmoud and C.M. Hirata, *Phys. Rev. D* **82** (2010) 063521.
- [79] Q. Yuan, B. Yue, X.-J. Bi, X. Chen and X. Zhang, *JCAP* **2010** (2010) 023.
- [80] M. Kuhlen, P. Madau and R. Montgomery, *Astrophys. J.* **637** (2006) L1.
- [81] W. Yang, S. Pan, S. Vagnozzi, E.D. Valentino, D.F. Mota and S. Capozziello, *JCAP* **2019** (2019) 044.
- [82] C.M. Hirata, *Mon. Not. Roy. Astron. Soc.* **367** (2006) 259.
- [83] B. Ciardi and P. Madau, *Astrophys. J.* **596** (2003) 1.
- [84] S.A. Wouthuysen, *Astron. J.* **57** (1952) 31.
- [85] X.-L. Chen and J. Miralda-Escude, *Astrophys. J.* **602** (2004) 1.
- [86] S.R. Furlanetto, *The 21-cm Line as a Probe of Reionization. In: Mesinger A. (eds) Understanding the Epoch of Cosmic Reionization. Astrophysics and Space Science Library*, vol. 423, Springer, Cham (2016).
- [87] J.-H. He and B. Wang, *Journal of Physics: Conference Series* **222** (2010) 012029.